Chapter 2

Micromachining Process and Basic Antenna Theory

There are two theoretical topics would be discussed in this chapter. One is the Micro-Electro-Mechanical technology, includes the process of Surface Micromachining, Bulk Micromachining and LIGA, each of them has their own advantages and applications. These processes are major steps in MEMS fabrication and are necessary process in Chapter 3 and Chapter 4. Another topic is the basic antenna theory of monopole antenna and leaky-wave antenna. The basic monopole antenna theory was used to design the flexible parylene and 3D micromachining antenna in Chapter 3 and Chapter 4. And in Chapter 5, the basic leaky-wave antenna theory was used to design a two–directional scanning method, where the short LWA is in top side and integrated with the aperture coupled patch antenna array on the other side of the substrate. Leaky-Wave Antennas occupy the advantages of frequency scanning capability, pencil-beam, easy matching, simple fabrication, and low profile.

2-1. Micro-Electro-Mechanical Technology

From a historical point of view, I would like to refer to a paper titled “There’s Plenty of Room at the Bottom” [1], which based on a seminar given in 1959 by the famous Nobel laureate physicist Richard Feynman. This paper is usually considered as the initial idea of the Microelectromechanical Systems (MEMS) technology. In that

paper, Dr. Feynman considered issues such as the manipulation of matter on an atomic scale and the feasibility of fabricating denser electronic circuits for computers. He also considered the issues of building smaller and smaller tools that could make even smaller tools so that eventually the individual atoms could be manipulated.

With the rapid growth and progress of the microelectronics technology which uses the single-crystal silicon as the basic material. The ability for realization of microstructure is well-established by using suitable integrated circuit (IC) process steps, such as thin film deposition, lithography, etching and so on. In the United States, such a micro-fabrication technology is known as MEMS, whereas in Europe, it is called microsystems technology (MST), and in Japan it is referred as micromachines.

MEMS technology is a multi-disciplinary technology, it includes radio frequency (RF MEMS), optical (Optical MEMS), chemistry, biology (BIO MEMS) [2] and other technologies [3]~[4]. Generally, it cab be categorized into three groups: surface micromachining, bulk micromachining, and LIGA (lithography, galvanoforming, moulding) [5]~[6]; each has their own advantages strengths weaknesses and applications [7] and will be discussed in the following subsections.

2-1.1 Surface Micromachining

Surface micromachining is a technology in which all functional features are built up on the surface of a substrate layer by layer [8]~[9]. This technique is based in deposition and patterning of thin film materials such as polysilicon, silicon nitride, or metallic thin film over a patterned sacrificial film such as silicon dioxide, polymer, or photoresist thin film. When the sacrificial layer is etched away, an undercut and freely suspended or movable structure can be obtained. The dimensions of these surface micromachined structures can be several orders of magnitude smaller than

bulk-micromachined structures. The prime advantage of surface-micromachined structures is their easy integration with IC components, since the wafer is also used for IC elements fabrication. It should be noted that as miniaturization is immensely enabled by surface micromachining, the small mass structure involved may be insufficient for a number of mechanical sensing and actuation applications [10].

Figure 2-1 shows the basic surface micromachining process. First a sacrificial layer is formed and patterned (Fig. 2-1a), followed by a similar process for the mechanical layer (Fig. 2-1b). Finally, the sacrificial layer is removed by sacrificial etching to leave the free standing structures (Fig. 2-1c). Note that the suitable sacrificial layer is dependent upon the mechanical layer used, with the important factor being the availability of an etchant which etches the sacrificial layer without significantly etching the mechanical layer or the substrate. The prime advantage of surface-micromachined structures is their easy integration with IC components, because the wafer is also the working area for IC elements.

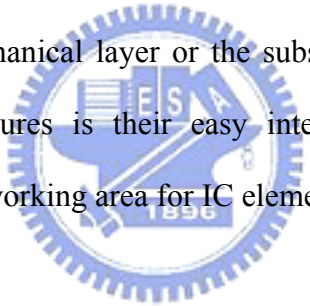

2-1.2 Bulk Micromachining

Bulk micromachining is the more mature one of the two silicon micromachining technologies. In bulk micromachining, structures are constructed by etching into a large single crystal substrate. Note that silicon is the most widely used material for substrate. The bulk micromachining technique can be divided into wet etching and dry etching of silicon according to the phase of etchants. Liquid etchants, almost exclusively relying on aqueous chemicals, are referred to as wet etching, while vapor and plasma etchants are referred to as dry etching. The term bulk micromachining comes from the fact that this type of micromachining is used to realize micromechanical structures within the bulk of a single-crystal silicon wafer by

selectively removing (‘etching’) significant amounts of silicon from the substrate to from membranes on one side of a wafer material. The microstructures fabricated using bulk micromachining may cover the thickness range from submicron to full wafer thickness (200 to 500 μm) and the lateral size range from submicron to the lateral dimensions of a full wafer [10].

Bulk micromachining technique allows to selectively removing significant amounts of silicon from the substrate to form membranes on one side of a wafer. Fig. 2-2 shows some typical bulk-micromachined structures [11]. Fig. 2-2 (a) and (b) show the isotropic and anisotropic etching in silicon substrate. These properties are defined by the nature of the chemical reactions, the diffusion of reactants and products, the additives, and other factors. By removing parts of the substrate, floating structures can be formed, as shown in Fig. 2-2 (c). Note that the etching stop layer is usually used in bulk micromachining technology to control the etching depth or construct the micro-structures, such as cantilevers and membranes.

By the combination of isotropic and anisotropic etching, robust structures can be built on or “in” the silicon wafers. Besides, by removing parts of the substrate, the performance of the RF device can be enhanced due to less substrate loss. Bulk micromachining technology now has attracted interest more in integration with complementary metal oxide semiconductor (CMOS) technology [12].

2-1.3 LIGA

LIGA is a German acronym standing for X-ray lithographie (X-ray lithography), galvanoformung (electroplating) and abformung (molding) [13]. The principal steps of the LIGA technology are shown in Fig. 2-3.

First, a thick photoresist is patterned with extend exposure to X-ray radiation, and the desired structures are formed after development (Fig. 2-3a). Metal is then electroplated on the exposed conductive surface of the substrate, filling the space and covering the top surface of the resist. After the photoresist is removed, the metal structure is formed Fig. 2-3b). Then, the metal structure is used as a mold insert for injection molding to form plating bases (Fig. 2-3c). The plating base replica is, in turn, used to electroplate additional metal parts, and is so-called second electroforming process (Fig. 2-3d). After removing the plastic part, the final product is formed.

The structures with high aspect ratio can be achieved by LIGA technique without the restriction of the crystal orientation. In addition, a large variety of materials are usable, like metals, ceramics, and polymers. The replication by micromolding offers the possibility of low cost mass production.

2-2. Basic Dipole Antenna Theory

In this section, we will discuss the theory for designing (a) dipole and monopole antenna, and also (b) meander line monopole antenna structure.

2-2.1 Dipole and monopole Antenna

The dipole antenna is one of the most basic antennas. The dipole antenna is basically a straight piece of wire cut in the center and fed with a balanced generator or transmission line [14]~[15]. The dipole antenna is often used with the size of half a wavelength ($l = \lambda/2$). This size is effective because when fed with RF power at the center point, the structure is resonant at the half wave frequency. For a $\lambda/2$ dipole antenna, the current distribution, $I(z)$, can be written as [15]:

$$I(z) = \mathrm{I_m} \sin\frac{2\pi}{\lambda}(\frac{\lambda}{4} - |z|)$$

$$= \mathrm{I_m} \sin(\frac{\pi}{2} - 2\pi\frac{|z|}{\lambda})$$

$$= \mathrm{I_m} \cos(2\pi\frac{z}{\lambda}) \qquad (2\text{-}1)$$

Where $\mathrm{I_m} = I(0)$ is the current magnitude at the feed point z = 0.

And its E-field can be written as:

$$\vec{E}(r,\theta) = \hat{a}_\theta\, j\eta_0\, \mathrm{Im}\frac{e^{-jk_0 r}}{2\pi r}\frac{\cos(\frac{\pi}{2}\cos\theta)}{\sin\theta} \qquad (2\text{-}2)$$

And the radiation intensity can be derived as follows:

$$U(r,\theta) = \frac{1}{2\eta_0}|E_\theta|^2$$

$$= (\frac{\eta_0|I_0|^2}{8\pi^2})(\frac{1}{r^2})\left[\frac{\cos(\frac{\pi}{2}\cos\theta)}{\sin\theta}\right]^2 \qquad (2\text{-}3)$$

Hence, the radiation power pattern of the λ/2 dipole antenna is:

$$P(\theta) = \frac{U(r,\theta)}{U\max}$$

$$= \left[\frac{\cos(\frac{\pi}{2}\cos\theta)}{\sin\theta}\right]^2 \qquad (2\text{-}4)$$

And the total radiated power, $\mathrm{P_{rad}}$, will be:

$$P_{rad} = \int_0^\pi \int_0^{2\pi} U(r,\theta) r^2 \sin\theta d\phi d\theta$$

$$= \frac{\eta_0|I_0|^2}{8\pi^2}\int_0^{2\pi} d\phi \int_0^\pi \frac{\cos^2(\frac{\pi}{2}\cos\theta)}{\sin\theta} d\theta$$

$$= \frac{1.22\eta_0}{4\pi}|I_0|^2 \qquad (2\text{-}5)$$

From equation (2-5), the radiation resistance, R_A, becomes:

$$R_A = \frac{2P_{rad}}{|I_0|^2} = \frac{1.22\eta_0}{2\pi}$$

The directivity of the antenna, D, then can be derived:

$$D = \frac{4\pi}{\int_0^{\pi}\int_0^{2\pi} P(\theta)\sin\theta d\phi d\theta}$$

$$= \frac{2}{\int_0^{\pi} \frac{\cos^2(\frac{\pi}{2}\cos\theta)}{\sin\theta} d\theta} \qquad (2\text{-}6)$$

Assume the efficiency of the λ/2 dipole antenna is 100 %, then the antenna gain, G, will be almost equal to D. Note that the antenna gain is a measure of how well the antenna radiates the RF power in a given direction, usually compared to a reference antenna, such as a dipole or an isotropic radiator. The gain is usually measured in dB's. A negative number means that the antenna in question radiates less than the reference antenna, a positive number means that the antenna radiates more.

By using equation (2-4), the radiation pattern of the λ/2 dipole antenna can be plotted as shown in Fig. 2-4. Note that it is not easy to draw a three dimensional radiation patterns, hence the three cross section profiles (x-y plane, y-z plane and x-z plane) are often used to demonstrate the radiation properties of the antenna.

A monopole is a dipole that has been divided in half at its center feed point and feed against a ground plane [14]. By using image theory, a monopole antenna can be equalized to a dipole antenna, as shown in Fig. 2-5. The dipole antenna is constructed with two metal elements that are symmetrically fed at the center by a balanced two-wire transmission line. One can understand the properties of a λ/4 monopole antenna by discussing the relative properties of the λ/2 dipole antenna. The charges

and currents on a monopole are the same as the upper half of its dipole counterpart, but the terminal voltage is only half of the dipole. Hence, the input impedance for a monopole antenna is half of its dipole counterpart, as shown in (2-7) [15]. Besides, the monopole can only radiate above the ground plane, and its radiation pattern is only the upper half of the dipole antenna, as shown in Fig. 2-6. Therefore, the λ/4 monopole antenna radiates only half as much power as the dipole antenna.

$$Z_{A,\,mono} = \frac{V_{A,\,mono}}{I_{A,\,mono}} = \frac{\frac{1}{2}V_{A,\,dipole}}{I_{A,\,dipole}} = \frac{1}{2}Z_{A,\,dipole} \qquad (2\text{-}7)$$

2-2.2 Meandered Structure

In order to reduce the size of the antenna, meandered configurations are usually used, as shown in Fig. 2-7 [16]. Thus, the meander line monopole antenna have vertical and horizontal segment. First, the input impedance is studied as a function of various numbers of segments as shown in Fig.2-8 [16]. Also shown in Fig. 2-8, the increase of the antenna length L_{ax} decreases the value of the first resonance frequency and increase the resonance impedance. The first-resonant frequency and impedance for various values of L_{ax} are derived from regression curve fit of the data plotted in Fig. 2-9.

When the total length of the antenna is fixed, the smaller line space, s, will result in more obvious EM-fields neutralizations of the horizontal segments. Hence, the resonant frequency is decreased. Besides, the narrower the line width, w, the lower the resonant frequency will be, due to its higher resonant impedance. The length shorting ratio (SR) is defined as equation (2-7), its value is suggested between 33 and 35% for computing the first resonance frequency of the meander line antenna [16]. More details about the meander configurations are discussed in references [17]~[19].

$$SR = \frac{\lambda/4 - L_{ax}}{\lambda/4} \qquad (2\text{-}7)$$

In general, the smaller the antenna, the radiation resistance, bandwidth and efficiency drops off, and tuning becomes increasingly critical. Hence, simply copying an existing design does not necessarily ensure reasonable performance. People who want to reduce the size of the antenna should consider the actual requirements for range, bandwidth and cost.

2-3. Theory of Leaky-wave Antenna

In this section, we will discuss the leaky mode of leaky-wave in microstrip line, and its radiation pattern and characteristics.

2-3.1 The leaky mode of leaky-wave in microstrip line

There are several wave modes propagate in a microstrip line on the substrates. The surface wave and a space wave are the two forms of leakage. The most convenient higher-order mode is the first higher mode (TE_{10}, leaky mode) [20] The first higher–order mode has a nonzero cutoff frequency, which depend on the guide width.. Dispersion curve for the lowest mode and the first two higher modes in microstrip line with a top cover is shown in the Fig. 2-10. The normalized phase constant β/K_0 is plotted against frequency. The solid lines represented real wave numbers, whereas the dashed lines correspond to the real parts of the leaky mode (complex) solution in “radiation region”. The microstrip line dimensions are strip W=3.0mm, dielectric layer thickness 0.6355mm and the height of the top cover is five times the dielectric layer thickness.

Hence, in order to perform a uniform leaky-wave antenna, we are employing a higher mode in an appropriate frequency range of operation. Fig. 2-11 shows the surface wave leakage in top view and cross view of microstrip line. The leakage away from the strip is the surface wave from on the dielectric layer outside of the strip region. The surface wave with phase constant $\vec{k}_s$, which has two components k_x and k_z in x direction and z direction, propagates away both sides of a micro-strip line at some angle. The field propagates axially (in the z direction) with phase constant β.

$k_x = 0$ $\beta \geq \vec{z} \cdot \vec{k}_s$ The wave is bounded in the microstrip line.

$k_x \geq 0$ $k_0 \leq \beta \leq \vec{z} \cdot \vec{k}_s$.

As $\beta < k_0$, small α, space wave become dominant part of the leakage power. When $\beta < k_0$, α increase larger, the wave is cutoff. The lowest mode on microstrip line is always purely bound, but the higher modes will leak the power away when the frequency is lowered below some critical value. When the open microstrip line is operated in its first higher mode, the electric field lines are roughly sketched. From the horizontal electric field polarization configuration on the top of the strip, it can be seen that radiation is expected to occur directly above the strip for this first higher mode. The leakage power is also expected in the form of surface wave. If the bulk of the leakage results in the space wave radiation, as happens in microstrip patch antennas, the structure can be used to be a practical antenna. In the next section, we will quickly extract the main features of the radiation characteristic once we know the β and α of the leaky mode.

We employed a rigorous (Wiener-Hopf) solution [21] to find the normalized complex propagation constant β/K_0-jα/K_0 of the first higher order mode, whereα/K_0 is normalized attenuation constant andβ/K_0 is normalized phase constant. The variation with frequency for a particular microstrip line of a dimension of line width 433mil for

a microwave substrate, ε_r =2.2 and H = 20mil, are plotted in Fig. 2-12. Moreover, the elevation angle θ between the main beam direction and end fire direction (the Z-axis direction) is calculated using the equation $\theta=\mathrm{Cos}^{-1}(\beta/\kappa_0)$. Hence, the angle θ is a function of frequency.

2-3.2 Microstrip Leaky Wave Antenna radiation considerations

Leaky wave antenna, as a special class of line source, are featured by normalized attenuation constant α/K_0 and normalized phase constant β/K_0. There are two aperture s along the microstrip line two edges, each of Length L and height h has leaky wave distribution are $\vec{E}_1(z)=\vec{x}Ae^{-\alpha z}e^{-j\beta z}$ and $\vec{E}_2(z)=-\vec{x}Ae^{-\alpha z}e^{-j\beta z}$ where A is a constant, respectively, which spaced a distance w. The far-zone electric fields of the leaky-mode antenna with length L can written as

$$E_r \cong E_\theta \cong 0$$

$$E_\phi \cong -jE_0\frac{khe^{-jkr}}{\pi\gamma}\left\{\sin\theta\left[\frac{\sin(X)}{X}\right]\left[\frac{e^{zL}-1}{z}\right]\right\}\cos\left(\frac{k\omega\sin\theta\sin\phi}{2}\right)$$

where

$$X = kh\sin\theta\cos\phi$$

$$Z = j(k\cos\theta-\beta)-\alpha$$

$$k=\frac{2\pi}{\lambda}$$

We assumed that there is no reflection from the far end of the leaky-mode antenna. Figure 2-13 shows each one of the two slots of microstrip line radiate into a half-space.

2-3.3 Characteristics of LWA

LWA are characterized by two specifications: the angle of maximum radiation θ_m, the half power beam width $\Delta\theta$. There exist simple equation θ_m relate and $\Delta\theta$ to normalized phase constant and the normalized attenuation constant.

(1) $\sin\theta_m \cong \frac{\beta}{k_0}$ and

(2) $\Delta\theta \cong \frac{1}{(\frac{L}{\lambda_0})\cos(\theta_m)}$. The length L is chosen so that 90% or so of the power is radiated. This length related to the normalized constant by

(3) $\frac{L}{\lambda_0} \cong \frac{0.183}{\frac{\alpha}{k_0}}$.

Physical meaning of variables of equation (1), (2), and (3) are shown in the following Fig. 2-14.

2-4. References

[1] Feynman, R. P., “There’s Plenty of Room at the Bottom,” Journal of Microelectromechanical Systems, Vol. 1, No. 1, 1992, pp. 60–66.

[2] Andreas Hierlemann, Oliver Brand, Christoph Hagleitner, and Henry Bltes: Microfabrication Techniques for Chemical/Biosensors, Proceedings of the IEEE, Volume 91, Issue 6, June 2003, pp. 839 – 863.

[3] Michael Pottenger, Beverley Eyre, Ezekiel Kruglick and Gisela Lin: MEMS: The Maturing of a New technology, Solid State Technology, Sept. 1997, pp. 89-86.

[4] Nadim Maluf and Kirt Williams: An Introduction to Microelectromechanical Systems Engineering, Second Edition, Artech House, Inc., Boston • London, 2004.

[5] S.M. Sze: Semiconductor Sensors, Wiley. 1994.

[6] Marc Madou: Fundamentals of Microfabrication, CRC Press, 1997.

[7] P. J. French and P. M. Sarro: “Surface versus bulk micromachining: the contest for suitable applications”, J. Micromech. Microeng., 8, 1998, pp. 45-53.

[8] C. Linder, L. Paratte, M.-A. Gratillat, V. P. Jaeklin and N. F. De Rooij: “Review Surface micromachining”, J. Micromech. Microeng., 2, 1992, pp. 122-132.

[9] P. J. French: “Topic Review Development of Surface Micromachining Techniques Compatible with On-Chip Electronics”, J. Micromech. Microeng., 6, 1996, pp. 376-384.

[10] Vijay K. Varadan, K. J. Vinoy, and K.A. Jose.: RF MEMS and their applications, New York: J. Wiley, 2003.

[11] Gregory T. A. Kovacs, Nadim I. Maluf and Kurt E. Petersen: “Bulk Micromachining of Silicon”, Proceedings of the IEEE, Volume 86, Issue 8, Aug.

1998, pp. 1536 – 1551.

[12] JackW Judy: “Microelectromechanical systems (MEMS): fabrication, design and applications”, Smart Mater. Struct. 10 (2001), pp. 1115–1134.

[13] Ehrfeld W et al 1987 “Fabrication of microstructures using the LIGA process”, Proc. IEEE Micro Robots Teleoperators Workshop (1987), Nov. 9-11, Hyannis, Cape cod, MA, USA.

[14] W. L. Stutzman and G. A. Thiele, Antenna Theory and Design, John Wiley & Sons, New York, Chapter 2, 1998.

[15] Balanis, Antenna Theory Analysis and Design, John Wiley & Sons, New York, Chapter 4, 1997.

[16] Lal Chand Godara, Handbook of Antenna in Wireless Communications, Boca Raton London New York Washington, DC, 2002, pp.12-8 - 12-40.

[17] M.Ali,S. S. Stuchly, and K. Caputa, “A wide-band dual meander-sleeve antenna”, J. Electromagnet., Waves and Appl., Vol. 10, No. 9, 1996, pp.1223-1236.

[18] H. Nakano, H. Tagami, A. Yoshizawa, and J. Yamauchi, “Shortening ratio of modified dipole antennas”, IEEE Trans. Antennas Propag, vol. AP-32, no.4, April, 1984, pp. 385-386,

[19] H.Y. Wang and M. J. Lancaster, “Aperture-coupled thin-film superconducting meander line antennas”, IEEE Trans. Antennas Propag, vol. 47, no.5, May 1999, pp. 829-836.

[20] A. A. Oliner, “A New Class of Scannable Millimeter wave antennas.” Proc. 20th European Microwave Conf. 1990, pp95-104.

[21] A. A. Oliner and K. S. Lee, “The nature of the leakage from Higher Modes on Microstrip Line,” 1986 IEEE Intl. Microwave Symp. Digest,pp.57-60, Baltimore, MD, June 1986.

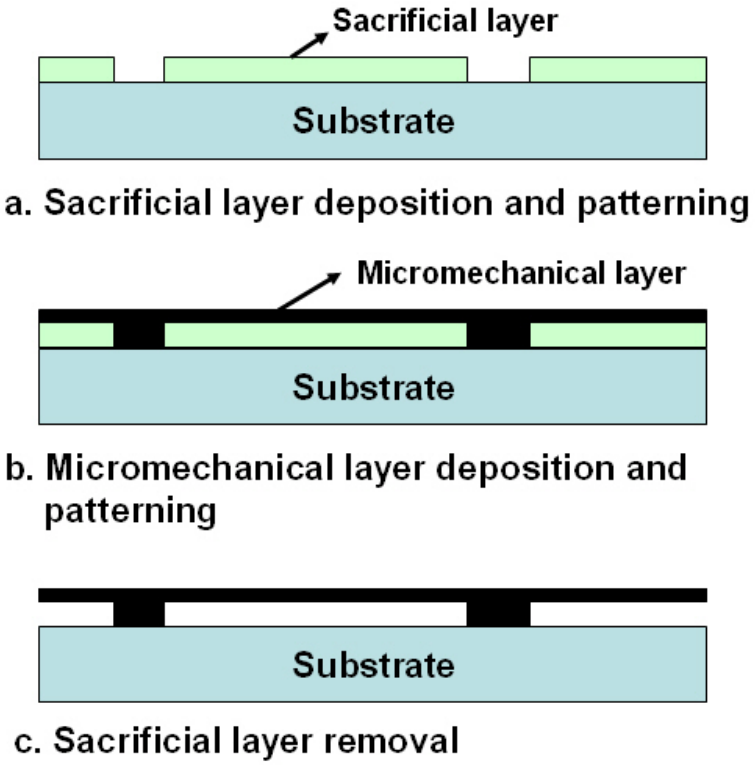

Figure 2-1: Schematic illustration of the basic process steps in surface micromachining.

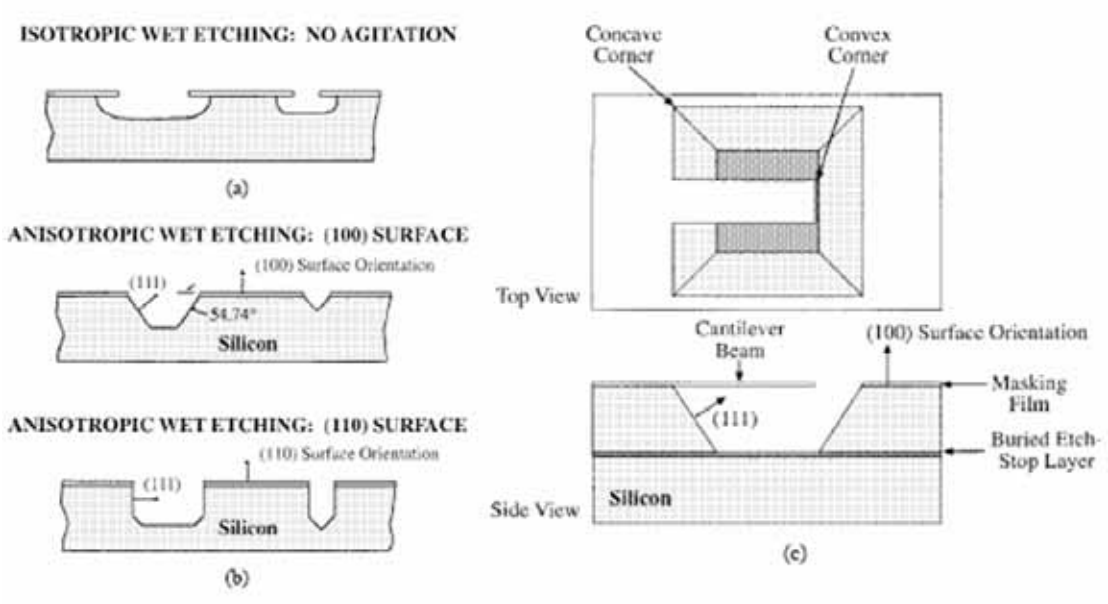

Figure 2-2: Illustration of possible bulk-micromachined structures.

(a) Rounded, isotropically etched pits in a silicon substrate.

(b) Pyramidal pits etched into (100) and (110) silicon using anisotropic wet etchants, bounded by (111) crystal planes.

(c) A pyramidal pit etched down to a buried etch-stop layer in (100) silicon, with an undercut cantilever beam. (2-4. [11])

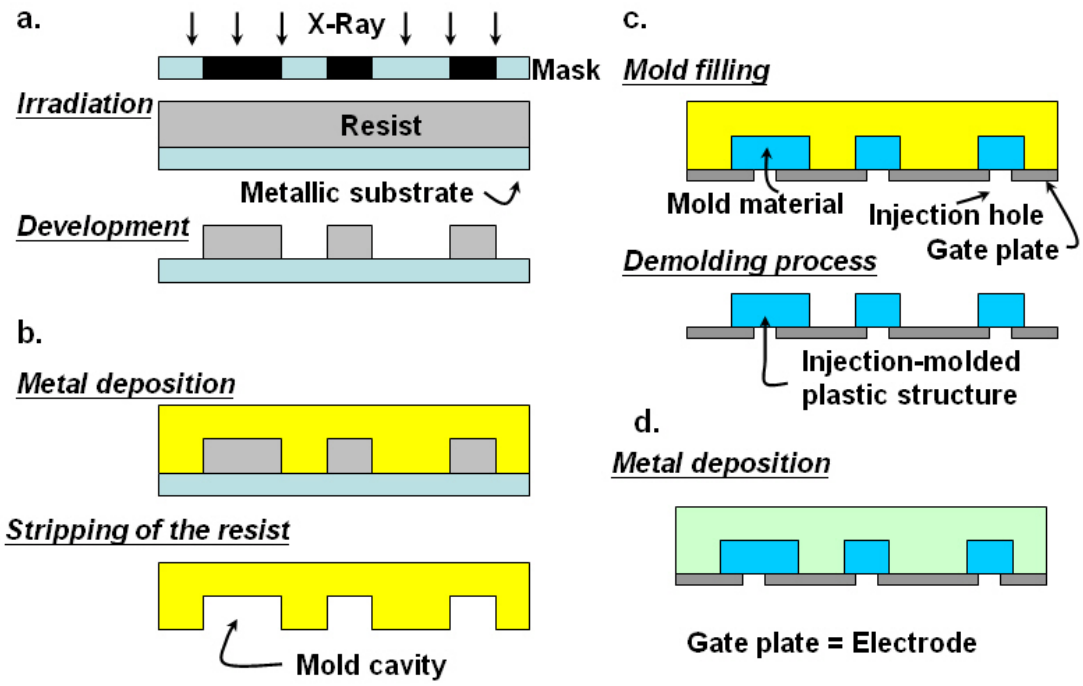

Figure 2-3: Typical sequence for the production of a microstructure based on the LIGA technique.

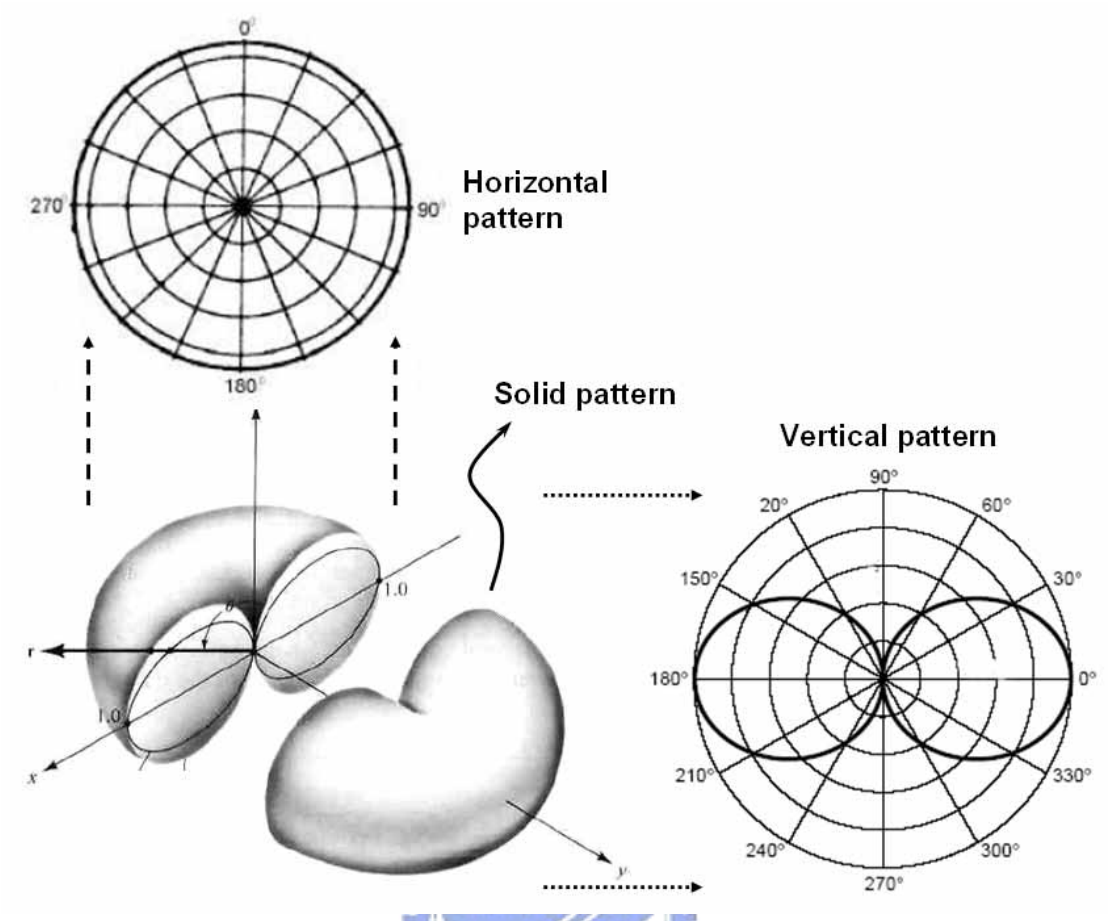

Figure 2-4: Three dimensional plot of the radiation pattern of the dipole antenna. (2-4. [15])

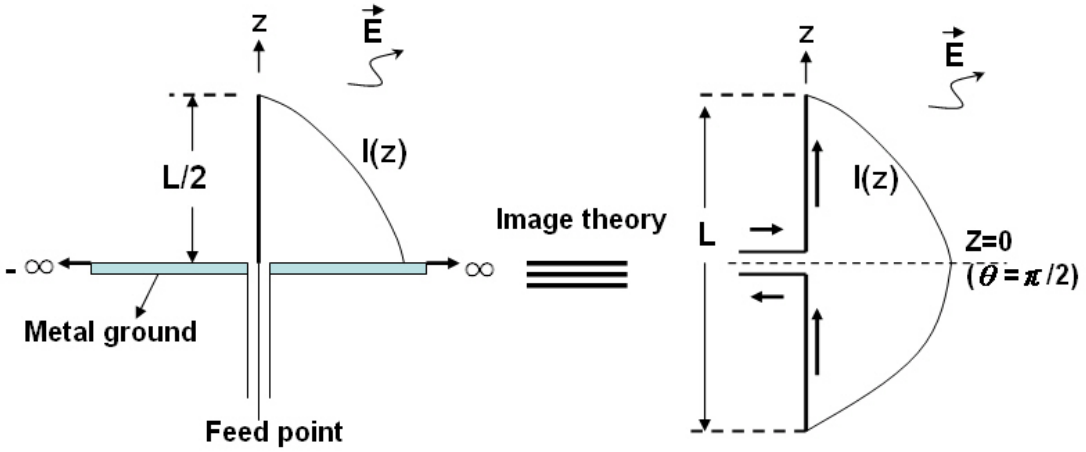

Figure 2-5: Current distribution of a monopole antenna and its equalized dipole antenna. (2-4. [15])

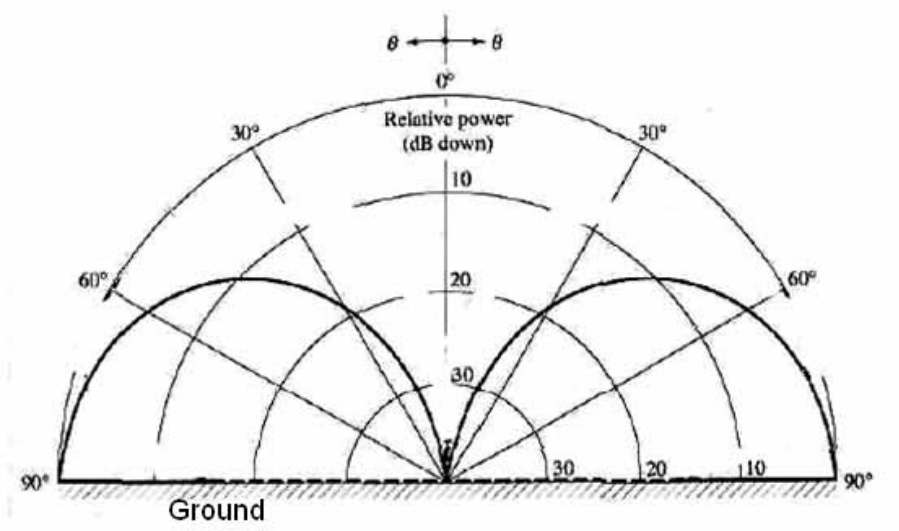

Figure 2-6: The radiation pattern of the ideal monopole antenna. (2-4. [15])

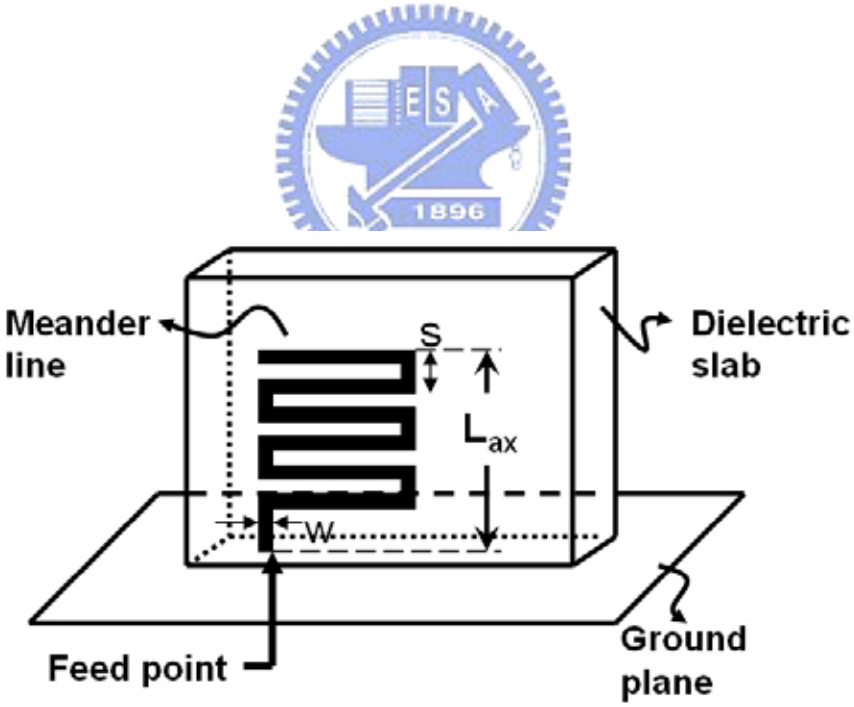

Figure 2-7: Meander line antenna with a finite ground plane. (2-4. [16])

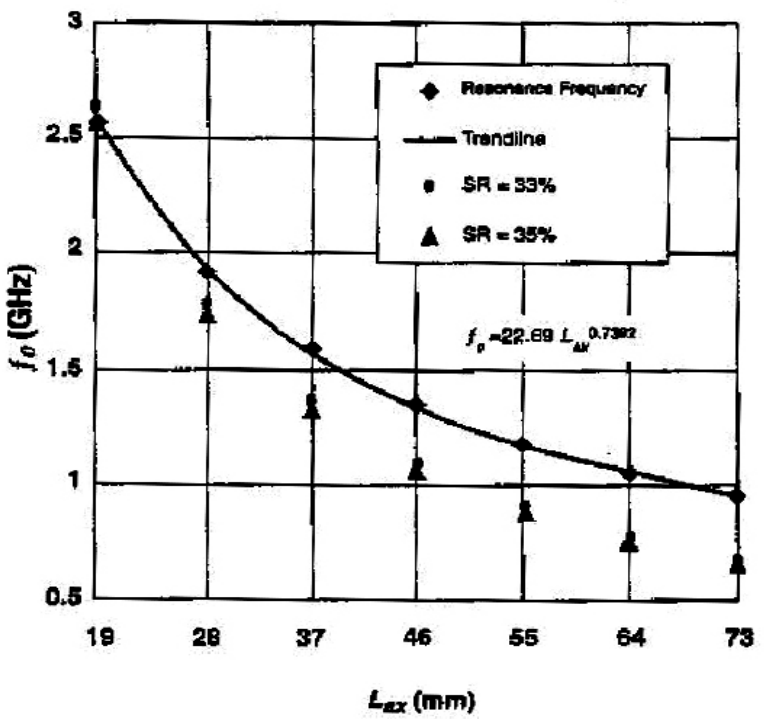

Figure 2-8: The frequency of a meander line antenna vs. L_{ax}. (2-4. [16])

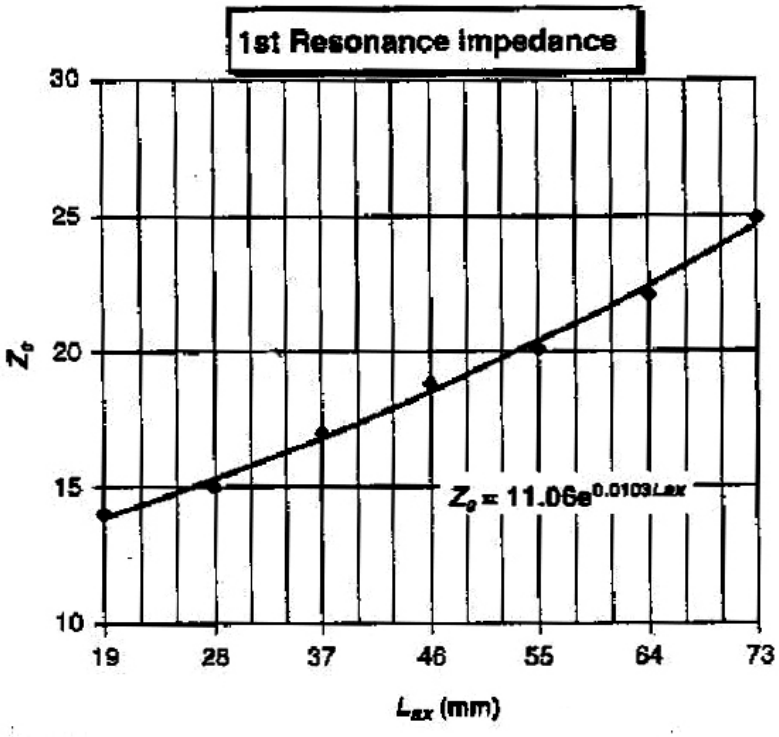

Figure 2-9: The impendence of a meander line antenna vs. L_{ax}. (2-4. [16])

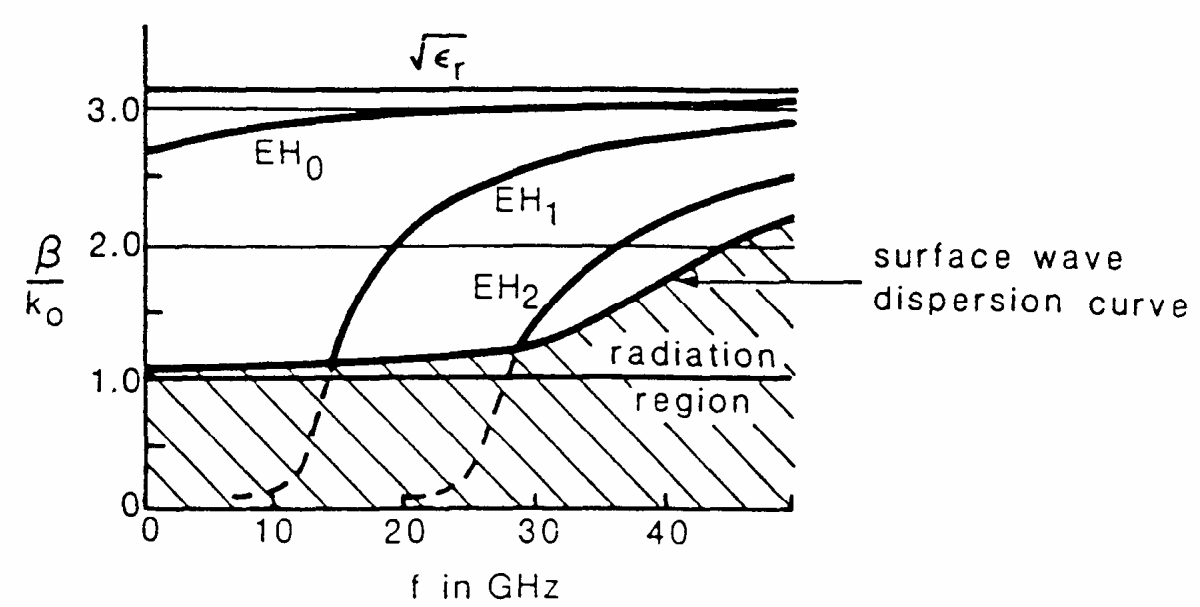

Figure 2-10: Dispersion curve for the lowest mode and the first higher modes in microstrip line with a top cover. The figure is copied from the A.A Oliner's paper. (2-4. [20])

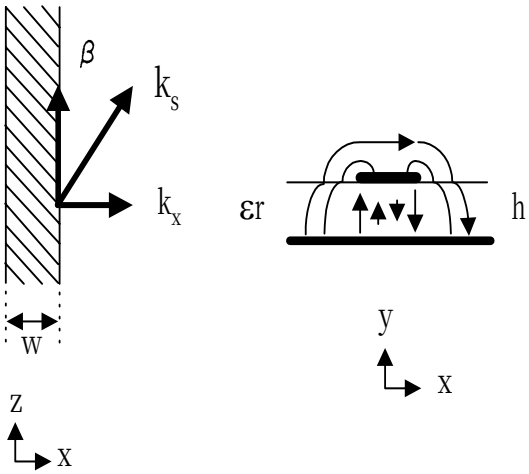

Figure 2-11: Top view and Rrough sketch cross view of open microstrip line operated in the first higher mode.

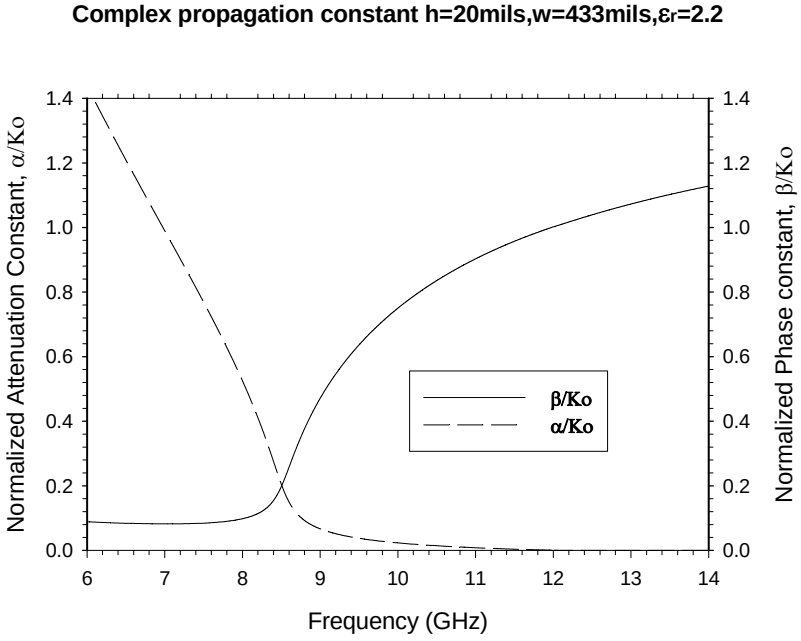

Figure 2-12: The variations of β/K_0 and α/K_0 with frequency for a particular microstrip line with W=433mil andε_γ=2.2 and H = 20mil. (2-4. [21])

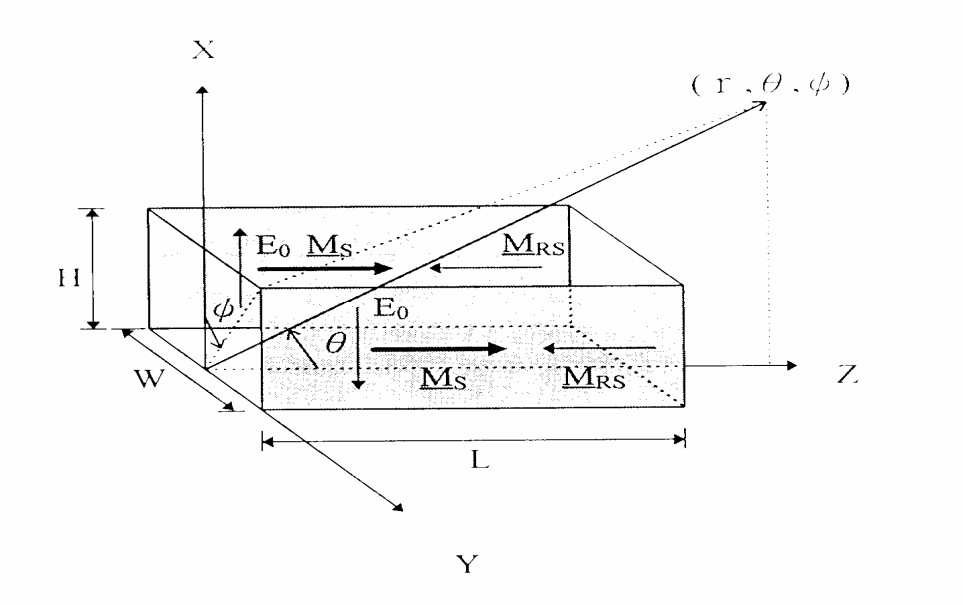

Figure 2-13: Geometry and coordinate system for the microstrip leaky-wave antenna.

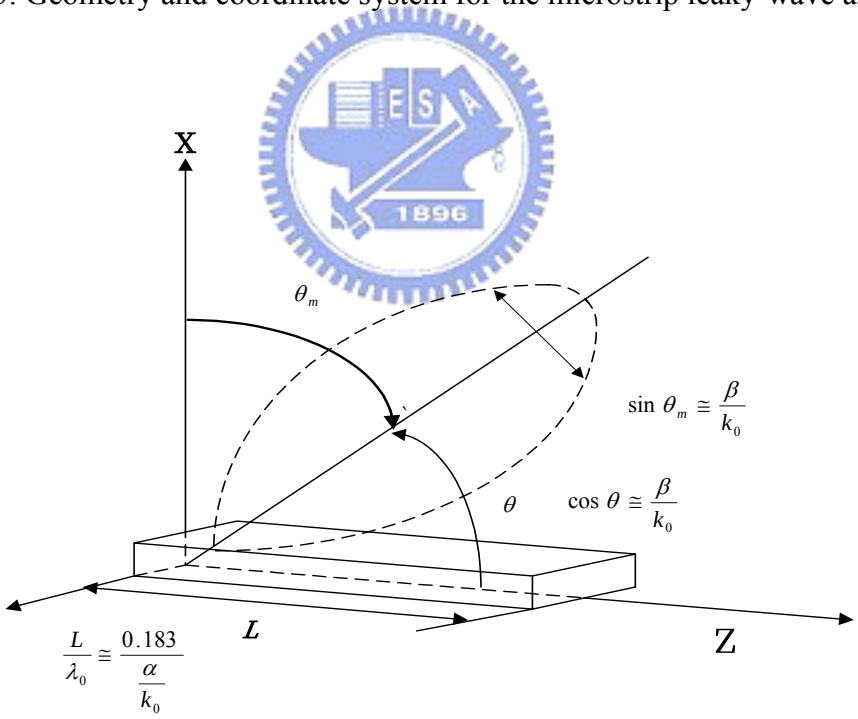

Figure 2-14: Coordinate system and the physical meaning of θ_m, and $\Delta\theta$.